CB-NOTE 274

Coupled channel analysis of the $\bar{p}p$-annihilation into $\pi^0\pi^0\pi^0$, $\pi^0\pi^0\eta$ and $\pi^0\eta\eta$ at rest and $\pi\pi$ scattering data

Stefan Spanier

University of Zürich

Abstract

The three pseudoscalar meson final states of $\bar{p}p$-annihilation at rest, $\pi^0\pi^0\pi^0$, $\pi^0\pi^0\eta$ and $\pi^0\eta\eta$ have been studied together with scattering data. These channels have shown to be suitable to extract information on the $I = 0$ and $I = 1$ S- and D-waves. In particular the existence of two $I^G(J^{PC}) = 0^+(0^{++})$ resonances was reported in a previous analysis using a N/D inspired method. The aim of the analysis presented here is to quantify the compatibility of the data samples with respect to the resonance hypotheses of the applied partial waves. To apply consequently the K-matrix formalism for the production process within the Isobar model for the $I = 0$ S-wave a 3×3 K-matrix had to be used.

1 Coupled channel analysis

All three data samples, $\pi^0\pi^0\pi^0$, $\pi^0\pi^0\eta$ and $\pi^0\eta\eta$ have been studied in the spirit of the Isobar model using the K–matrix formalism [1, 2, 3]. The final state interaction of $\bar{\text{p}}$p-annihilation at rest into three mesons is considered as a production of a resonance in a two body scattering system and a recoil particle. The extension of the scattering to production processes is done using the P-vector approach suggested by Aitchison [4]. The formalism is based on the K-matrix. This formalism has the advantage, that partial waves of equal quantum numbers $I^G(J^{PC})$ in different final states of the $\bar{\text{p}}$p-annihilation can be coupled. Since the two-body reaction amplitude T is also based on the K-matrix, scattering data can also be included. Resonances appearing in the different decay modes are considered in the same underlying K-matrix. Hence the number of parameters is reduced. In addition one makes stronger statements about the production and decay of resonances compared to the separate analyses of the final states. The figure shows a representation of the Isobar model amplitudes.

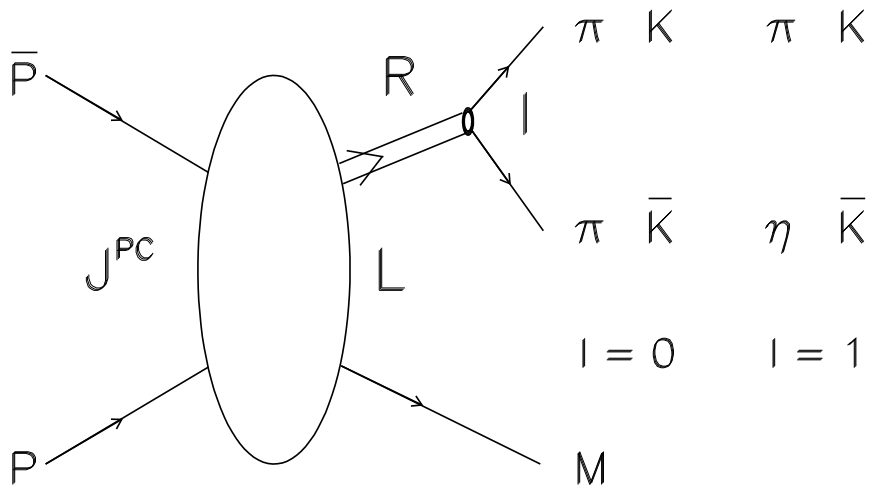

1.1 Transition amplitude

Neglecting isospin for the analysis of the final states consisting of three neutral pseudoscalar mesons the following total transition amplitude is used:

$$A_{J^{PC}}(\vec{p},\vec{q}) = \sum_{\text{symmetr}} Z_{J^{PC},l,L}(\vec{p},\vec{q}) \cdot D_L(p) \cdot F_l(q) \qquad (1)$$

It describes the transition from a definite initial state J^{PC} of the $\bar{\text{p}}$p system into the three body final state. The final state is described by l, L (L = angular momentum

between the isobar and the recoil meson of momenta $\pm\vec{p}$; l = angular momentum of the isobar splitting into two mesons of momenta $\pm\vec{q}$). Symmetrization is done by summation over the permutations of the identical bosons. The following notation is used:

$A_{J^{PC}}(\vec{p},\vec{q})$	:	partial wave amplitude
$Z_{J^{PC},L,l}(\vec{p},\vec{q})$	:	spin-parity function
$D_L(p)$	:	centrifugal barrier of the di-meson production with relative angular momentum L written as a quotient of Blatt-Weisskopf factors [5]
$F_l(\vec{p},\vec{q})$	:	dynamical function

The density of Dalitz plot entries I_k (I_k = intensity per Dalitz plot cell at (m_{12}^2, m_{13}^2)) is given by the incoherent sum of the densities of contributing initial states:

$$I_{k,theo} = \sum_{J^{PC}} |A_{k,J^{PC}}|^2 \tag{2}$$

From this the χ^2 is derived for a binned Dalitz plot:

$$\chi^2 = \sum_{k=1}^{cells} \frac{(I_{k,theo} - I_{k,exp})^2}{\sigma_{I_k}^2} \tag{3}$$

The error $\sigma_{I_k}^2$ is the sum of the statistical error per cell $\sigma_{k,exp}$ and a theoretical error $\sigma_{k,sys}$, where $\sigma_{k,theo} \ll \sigma_{k,exp}$, since a large number for calculation of the amplitudes was used. The systematics is tested by different hypotheses and different representations of the data.

1.1.1 Spin-parity function

For the formulation of the transition via intermediate resonant states with a certain spin the formalism of Zemach[6] was used. Intermediate states with angular momentum less than 3 are taken into account. In the coupled channel analysis it is assumed that the possible initial states from wich annihilation can take place is $^1S_0$ only.

initial state	$\pi^0\pi^0$ (l)	rec (L)	$\pi^0\eta$ (l)	rec (L)	angular distribution
$^1S_0$ (0^{-+})	0	0	0	0	1
			1	1	$\cos^2\theta$
	2	2	2	2	$(\cos^2\theta - \frac{1}{3})^2$

The construction of the tensors is based on the momentum vectors $\vec{p}$ and $\vec{q}$. The following normalization was used: $\vec{p}\cdot\vec{q} = cos\Theta$.

1.1.2 Dynamical function

In the Isobar model a two particle resonance is produced while the other particles play the role of spectators. The final state interaction can be treated like a scattering process. The resonance propagator in the simplest case of a well separated single channel resonance is a Breit-Wigner function. But for overlapping resonances the sum of these amplitudes violates unitarity. The S–operator is written as a sum of the unity matrix and the reaction matrix T:

$$S = \mathbb{1} + 2i\rho T \tag{4}$$

ρ is the two body phase space; $\rho_i = \frac{2q_i}{M}$. q_i is the breakup momentum of channel i:

$$q_i(M_i) = \frac{\sqrt{(M_i^2 - (m_{i_1} + m_{i_2})^2)(M_i^2 - (m_{i_1} - m_{i_2})^2)}}{2M_i} \tag{5}$$

To ensure the unitary of S the T–matrix can be written in terms of the K–matrix. For S unitary K is hermitian. Time reversal invariance for S means that K is real and symmetric.

$$T = (\mathbb{1} - iK\rho)^{-1}K = K(\mathbb{1} - i\rho K)^{-1} \tag{6}$$

In resonance approximation the K–matrix can be parametrized as:

$$K_{ij} = \sum_{\alpha} \frac{g_{\alpha i} g_{\alpha j} D^l_{\alpha i}(q, q_\alpha) D^l_{\alpha j}(q, q_\alpha)}{m_\alpha^2 - m^2} + c_{ij} \tag{7}$$

with

m_α	:	K-matrix pole position
$g_{\alpha i}$	:	coupling strength of the α pole to the ith channel
$D^l_{\alpha i}(q, q_\alpha)$	:	centrifugal barrier
c_{ij}	:	real background constant

The coupling strength $g_{\alpha i}$ can be given as

$$g_{\alpha i} = \sqrt{\frac{m_\alpha \Gamma_{\alpha i}}{\rho_i(m_\alpha)}}. \tag{8}$$

The $\Gamma_{\alpha i}$ are parametrizations of the partial widths of K–matrix pole m_α. The term $(\mathbb{1} - iK\rho)^{-1}$ can be identified as a generalization of the resonance propagator within a partial wave, via which the initial state scatters into the final state. To ensure that the amplitude arrives at zero at the $\pi\pi$ threshold the K–matrix in eqn. 7 is multiplied by a factor $f = (m^2 - 2m_\pi^2)/m^2$.

For production (annihilation) processes the initial state is not part of the scattering states. According to Aitchison[4] the production of resonances is described by the production vector P which incorporates the same poles as the K–matrix. The

coupling $g_{\alpha i}$ to the initial state transforms into a production strength β_α for the resonance.

$$P_i = \sum_\alpha \frac{\beta_\alpha \, g_{\alpha i} D^l_{\alpha i}(q, q_\alpha)}{m_\alpha^2 - m^2}. \tag{9}$$

The dimensionless production strength β^0_α is obtained by

$$\beta_\alpha = \beta^0_\alpha \sqrt{\sum_i g^2_{\alpha i}}. \tag{10}$$

The dynamical function (now a vector) is given as (l omitted):

$$F = (I - iK\rho)^{-1} P \tag{11}$$

In the simple case of one resonance, one open channel (spin 0) the F reduces to a relativistic Breit-Wigner function:

$$F = \beta_0 \frac{e^{i\delta}}{\rho} \sin\delta = \frac{m_0 \Gamma_0 / \rho(m_0)}{m_0^2 - m^2 - i m_0 \Gamma(m)} \tag{12}$$

where the energy dependent width is given as:

$$\Gamma(m) = \Gamma_0 \frac{\rho(m)}{\rho(m_0)} \tag{13}$$

In that case the K–matrix pole and the resonance position are identical. In general the K–matrix pole position m_α and its decay widths $\Gamma_{\alpha i}$ is not the physical pole position. This is obtained in the complex energy plane from the corresponding T–matrix.

1.2 Model

The creation of the observed final states results in two steps: First the production of the resonance and the spectator particle, second the decay of the resonance in the two-body scattering system well separated from the primary production.

The spectator meson S marks the kind of production of the resonance R. For a process

$$\begin{aligned} \bar{\mathrm{p}}\mathrm{p} &\rightarrow RS \\ &\hookrightarrow \pi\pi \\ &\hookrightarrow \eta\eta \end{aligned} \tag{14}$$

one expects the same production but different couplings to the final state described by $\Gamma_{\pi\pi}$ and $\Gamma_{\eta\eta}$. For the processes

$$\begin{aligned} \bar{\mathrm{p}}\mathrm{p} &\rightarrow RS \\ &\quad RS' \end{aligned} \tag{15}$$

Table 1: Data samples

channel	B.R. / $\times 10^{-3}$	events	ϵ_{rec}	binning / MeV$^2\times$ MeV^2	cells
$\pi^0\pi^0\pi^0$	6.2 ± 1.0	712114	0.302 ± 0.016	26666.7 $\times$ 26666.7	1338
$\pi^0\pi^0\eta$	6.7 ± 1.2	374340	0.284 ± 0.025	28526.31 $\times$ 28526.31	1738
$\pi^0\eta\eta$	2.0 ± 0.4	30958 166621 (trig)	0.257 ± 0.027	18582.72 $\times$ 18582.72	1798

production is differently. So one should a priori not imply that the production parameters are the same.

If one corrects the data sample for its branching ratio in the $\bar{p}p$-annihilation at rest a resonance is produced with a strength β and then couples differently to the final states. Therefore in the second case only the production phases may differ for the two reactions where in the first case eqn. 14 also this parameter is fixed. A hint for a differently produced resonance is $f_0(980)$ seen in $\pi^0\pi^0\eta$ and $\pi^0\pi^0\pi^0$: In $\pi^0\pi^0\eta$ recoiling against an η it appears as a peak, in $\pi^0\pi^0\pi^0$ produced against π^0 it appears as a dip. If the same resonances propagate the denominator of the production amplitudes F_i and the T_{ij} are the same.

2 Data samples

The preparation of the final states with three pseudoscalar mesons is described elsewhere[7, 8, 9, 10]. The parameters of the used data-samples are given in table 2. The number of cells is the relevant number of data-points. For the $\pi^0\eta\eta$ data sample data from the 6γ set and triggered data were combined. This is justified by the χ^2 comparison of the binned data sets performed in[10] ($\chi^2 = 1.08$). The Dalitz plots are displayed in fig. 1. The scattering data were taken from[11, 12] and are shown in fig. 2.

To determine the reconstruction efficiency and acceptance variation the final states were simulated by CBGEANT (version 4.06/07): 280,000 events for $\pi^0\pi^0\pi^0$, 470,000 events for $\pi^0\pi^0\eta$ and 400,000 events for $\pi^0\eta\eta$. For the three samples the acceptance is nearly uniform over the whole phase space. Variations enter into the efficiency. The acceptance distribution over the Dalitz plot is smoothed with angular distributions without any two body dynamics using the same fit program as for the partial wave analysis. Dalitz plot cells are corrected for the appropriate acceptance before they enter into the fit. The area for bins crossing the Dalitz plot boundary is corrected.

The errors of fitted parameters in the coupled channel analysis were determined using MINUIT errors but also different binnings of the Dalitz plots (table 2), fits with and without acceptance correction and boundary bins.

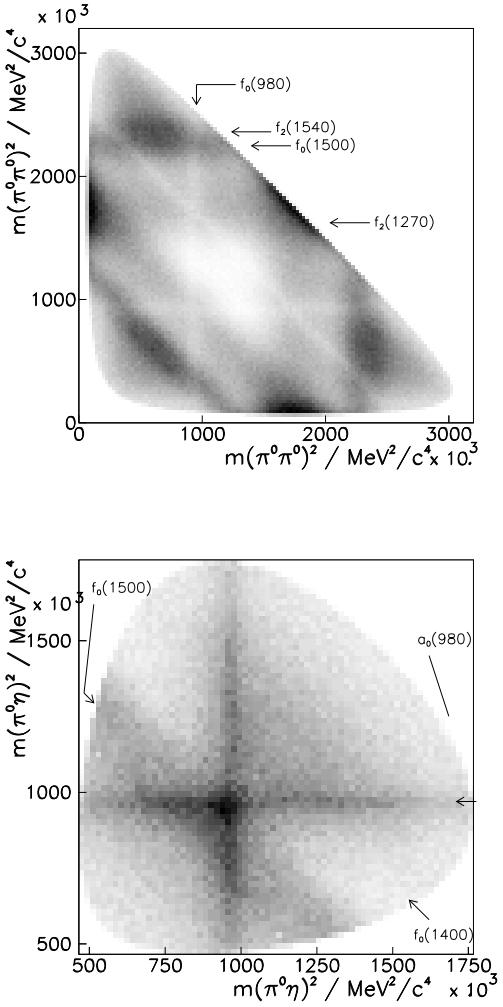

Figure 1: Dalitz plot for the reactions (1) $\bar{p}p \to \pi^0\pi^0\pi^0$, (2) $\bar{p}p \to \pi^0\pi^0\eta$ and (3) $\bar{p}p \to \pi^0\eta\eta$.

Table 2: Data samples systematics

channel	binning	acceptance	areacorr
$\pi^0\pi^0\pi^0$	120, 100	$\pm$	$\pm$
$\pi^0\pi^0\eta$	90, 80	$\pm$	$\pm$
$\pi^0\eta\eta$	70,65	$\pm$	$\pm$

3 Coupled fit

Which information can be combined ? An overview of the accessible S and D–waves contains table 3.

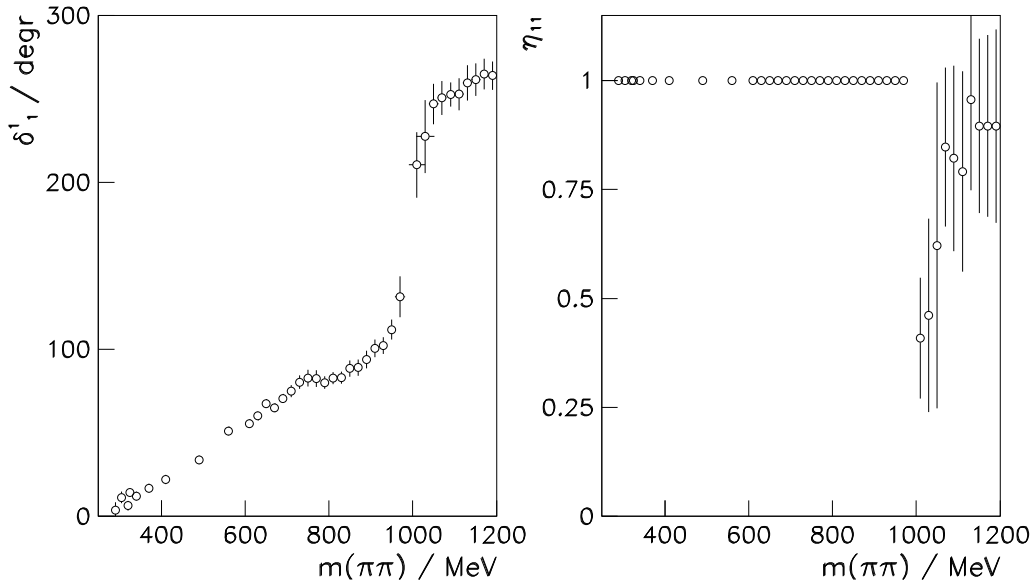

Figure 2: Scattering data taken from the CERN-Munich and the K_{e4} decay experiment.

Table 3: S and D waves which can be combined.

data	S,D-waves	phase space / MeV
$\pi^0\pi^0\pi^0$	$\pi\pi$	270 ... 1740
$\pi^0\pi^0\eta$	$\pi\pi$	270 ... 1330
	$\pi\eta$	680 ... 1740
$\pi^0\pi^0\pi^0$	$\eta\eta$	1095 ... 1740
	$\pi\eta$	680 ... 1330
$\pi\pi$ scat.	$\pi\pi$	280 ... 1200

3.1 The $I = 0$ S-wave

data	resonances	couplings		
		$\pi\pi$	$\bar{\mathrm{K}}\mathrm{K}$	$\eta\eta$
$3\pi^0$	$f_0(980), (f_0(1100)), f_0(1360), f_0(1500)$	x	x	
$\pi^0\pi^0\eta$	$f_0(980), f_0(1360)$	x	x	
$\pi^0\eta\eta$	$f_0(1360), f_0(1500)$		x	x
$\pi\pi$ scat	$f_0(980), (f_0(1100))$	x	x	

To describe the $\pi\pi$ S–wave from threshold up to 1.2 GeV at minimum two K–matrix poles and one background constant c_{12} is needed [13]. The constants c_{11} and c_{22} are redundant.

In $3\pi^0$ the $\pi\pi$ S–wave is described alternatively by three or four K–matrix poles. The $f_0(980)$ and a $f_0(1500)$ are clearly seen in the Dalitz plot and are needed in any description of the data. Their pole positions depend only weakly on the particular choice of fit amplitudes. The low energy part of the $\pi\pi$ S-wave needs a K–matrix pole at $m_1 = 840\,\mathrm{MeV}$ and a second one at about $m_2 = 1200\,\mathrm{MeV}$. The second pole parametrizes the steady increase of the $\pi\pi$ phase shift over the full energy range. Fits using this parametrization were unsatisfactory. A third K–matrix pole at about 1560 MeV is necessary to describe the $f_0(1500)$. In addition to $f_0(980)$ and $f_0(1500)$ one finds a Breit-Wigner pole at 1330 MeV having a large width ($\Gamma \approx 600\,\mathrm{MeV}$). The solution with four poles in the K–matrix differs in two ways from the previous one in physics: The width of the resonance at 1330 MeV reduces to $\Gamma = (300 \pm 80)\,\mathrm{MeV}$ and an additional pole at 1100 MeV (average of sheet III and sheet II) is found. The parameters of the $f_0(980)$ and $f_0(1500)$ are stable. The difference in χ^2 between the two solutions is small. The $\pi^0\eta\eta$ data set asks for two poles above the $\bar{\mathrm{K}}\mathrm{K}$ threshold. The description of the $\pi^0\eta\eta$ final state revealed an $f_0(1360)$ and a $f_0(1500)$[10] or $f_0(1560)$[14]. The mass shift between the two latter is caused by the different dynamical functions. In[14] the sum of Breit-Wigner functions was used which causes a mass shift against the poles in the T–matrix parametrized via K–matrix[15]. The combination of the data sets enforces four poles. Further poles in the $\pi\pi$ S–wave destabilize the fit or pushed far out of the avaible phase space.

To combine the information of the data sets a 3×3 K–matrix is set up. The eqn. 7 written in form of the couplings:

$$K_\alpha = \frac{1}{m_\alpha^2 - m^2} \begin{pmatrix} g_{\pi\pi}^2 & g_{\pi\pi} g_{\bar{\mathrm{K}}\mathrm{K}} & g_{\pi\pi} g_{\eta\eta} \\ g_{\bar{\mathrm{K}}\mathrm{K}} g_{\pi\pi} & g_{\bar{\mathrm{K}}\mathrm{K}}^2 & g_{\bar{\mathrm{K}}\mathrm{K}} g_{\eta\eta} \\ g_{\eta\eta} g_{\pi\pi} & g_{\eta\eta} g_{\bar{\mathrm{K}}\mathrm{K}} & g_{\eta\eta}^2 \end{pmatrix} \tag{16}$$

where $K = \sum_\alpha K_\alpha$. The g_i are the coupling strengths of pole m_α. The coupling to $\bar{\mathrm{K}}\mathrm{K}$ parametrizes the observations at $\bar{\mathrm{K}}\mathrm{K}$ threshold. Since this channel is not observed directly it provides a general inelasticity.

3.2 $I = 1$ S–wave

The resonance features of the $\pi\eta$ S–wave probed in $\pi^0\pi^0\eta$ and $\pi^0\eta\eta$ are the $a_0(980)$ and the $a_0(1470)$.

data	resonances	couplings	
		$\pi\eta$	$\bar{\mathrm{K}}\mathrm{K}$
$\pi^0\pi^0\eta$	$a_0(980), a_0(1470)$	x	x
$\pi^0\eta\eta$	$a_0(980), (a_0(1470))$	x	x

Here a 2×2 K–matrix is used as in[3].

3.3 $I = 0$ D–wave

data	resonances	couplings	
		$\pi\pi$	$\eta\eta$
$\pi^0\pi^0\pi^0$	$f_2(1270), f_2(1540)$	x	
$\pi^0\eta\eta$	$f_2(1525)$		x

To preserve unitarity for each of the two final states a 1×1 K–matrix is applied. It was tested if the high mass tensor resonance can be coupled to $\pi\pi$ and $\eta\eta$ by using a 2×2 K–matrix. This procedure destabilized the fit and the width of the pole went to values above 300 MeV . In the table above already the meson interpretation of the resonances is implicated.

3.4 $I = 1$ D–wave

The $a_2(1320)$ in a separate fit to $\pi^0\eta\eta$ contributes up to 3%. For the coupled channel analysis the D-wave obtained in the investigation of $\pi^0\pi^0\eta$ is used. The parametrization is done by a 1×1 K–matrix. The fit revealed a contribution of $a_2(1320)$ to the $\pi^0\eta\eta$ final state of less than 1%. The results on $\pi^0\pi^0\eta$ are unchanged.

3.5 $I = 1$ P–wave

For the description of the $\pi^0\pi^0\eta$ final state the P–wave is introduced as described in[3].

3.6 Choice of the initial states

Fits assuming that $^1S_0$ protonium initial state contributes only lead to acceptable descriptions in all three data samples: $\chi^2 = 2426/(1338\text{-}27)$ in $3\pi^0$ with a four-pole solution, but no systematic deviations between data and fit; $\chi^2 = 1.44$ in $\pi^0\eta\eta$, where the introduction of $a_2(1320)$ in parallel to the introduction of transitions from P–states improved χ^2 to 1.32. A χ^2 of about 1.3 was achieved under this hypothesis for the $\pi^0\pi^0\eta$ final state.

It is well known that annihilation in liquid hydrogen occurs preferentially in S-states of the protonium [16]. For the coupled channel fits it is assumed that annihilation takes place from the $^1S_0$ initial state of the $\bar{p}p$ atom; possible contributions from P–state annihilation are neglected. This also helps to keep the number of parameters small and allowed stable fits.

3.7 Correction of the data-samples

Each data sample was corrected for acceptance and phase space area. Before one is able to ask for common production strengths of resonances seen in different final states one has to correct the number of events to the ratio in $\bar{p}p$ annihilation at rest

and for the data representation. To each Dalitz plot the correction factor eqn. 17 was applied. It is normalized to the $3\pi^0$ Dalitz plot.

$$corr = \frac{bin(3\pi^0)}{bin(x)} \frac{1}{\epsilon_{rec}} \cdot [\alpha_{sampling}][\frac{1}{\pi^0 \to \gamma\gamma}\cdot]^m[\frac{1}{\eta \to \gamma\gamma}\cdot]^n \tag{17}$$

$bin(3\pi^0)$	:	length of an edge of a cell in $3\pi^0$
$bin(x)$	:	bin edge length of plot x
ϵ_{rec}	:	reconstruction efficiency
$\alpha_{sampling}$	:	correction of the number of data for triggered samples
$\pi^0 \to \gamma\gamma$	:	$[]^n$ optional for m π^0 (0.988)
$\eta \to \gamma\gamma$	:	$[]^m$ optional for n η (0.388)

For the data samples described in table 2 one obtaines $corr = 3.43$ for $3\pi^0$, $corr = 8.69$ for $\pi^0\pi^0\eta$ and $corr = 5.89$ for $\pi^0\eta\eta$. Of course the χ^2 is not influenced by the manipulations of the entries per Dalitz plot cell. That the fit program handles the different data samples correctly was tested with simulated Dalitz plots (see appendix).

The data samples consist of different numbers of data points and derived from different experiments. Before adding the χ_i^2 one therefore has to scale them.

$$\chi^2 = \sum_i f_i \cdot \chi_i^2 \tag{18}$$

The choice of the f_i was done with respect to the scattering data (39 data points, $f_i = 1$) and in accordance with the scalings used in the individual analyses of the Dalitz plots together with scattering data. For the calculation over the whole Dalitz plots $f_{3\pi^0} = 1/10..1/30$ (1338 cells), $f_{\pi^0\pi^0\eta} = 1/40..1/60$ (1738 cells) and $f_{\pi^0\eta\eta} = 1/40..1/60$ (1798 cells). Within the given ranges these factors ensured nearly compatible χ_i^2. The number of parameters varied for the common description of the four data samples is 45.

4 Fit

The fit was performed with the same program which was used for the analyses of the individual plots[3, 2, 1]. It is based on the well established MINUIT-package[17] of CERN. The program was run on DEC-Alpha (VMS and OSF/1) and DEC-stations (ULTRIX). Double precision calculations were performed.

The best fit arrived at the following χ_i^2 (given with the relevant number of data points):

- $\pi^0\pi^0\pi^0$: 2448 / 1338
- $\pi^0\pi^0\eta$: 2657 / 1738
- $\pi^0\eta\eta$: 2896 / 1798
- $\pi\pi$ scat : 46 / 39

To study the variations of parameters the common hypothesis was applied to each plot separately, too. In practice the scaling factors of the χ^2 of the remaining two Dalitz plots were set to zero. This led for $3\pi^0$ to $\chi^2 = 2355/1338$, for $\pi^0\pi^0\eta$ to $2257/1738$ and for $\pi^0\eta\eta$ to $2661/1798$. The comparison between fit and data is given in the following subsections.

Of course for features attributed to common dynamics the fit tries to find the average for the descriptive parameters. Since we have data samples from different experiments with different resolutions and one has different structures of the partial waves (especially the $I = 0$ S–wave, where $f_0(980)$ is seen as dip or as a bump) with the same resonance pattern one expects a decrease in the quality of the fit compared to the individual analyses. Especially at sharp edges (as seen at $\bar{\mathrm{K}}\mathrm{K}$ threshold in $\pi^0\pi^0\eta$ or the $a_0(980)$ in $\pi^0\eta\eta$) deviations can appear. In the representation of data and fit the Monte Carlo resolution is not taken into account. At 1 GeV it is about 8 MeV. This is forseen in the appropriate binning of the data. In summary the common description of the data is reasonable good.

4.1 $3\pi^0$

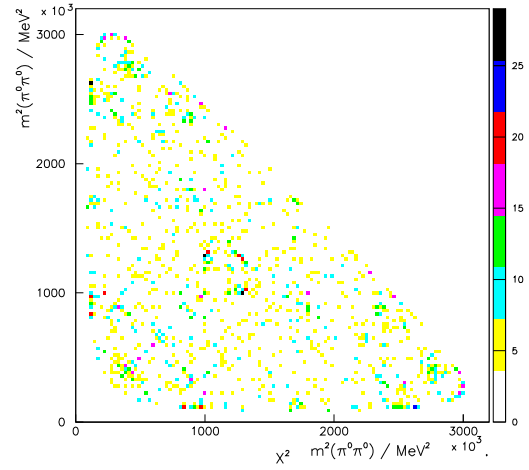

Figure 3:
The chisquare-plot for $3\pi^0$. Deviations occur at the high mass boundary where acceptance correction plays an important role.

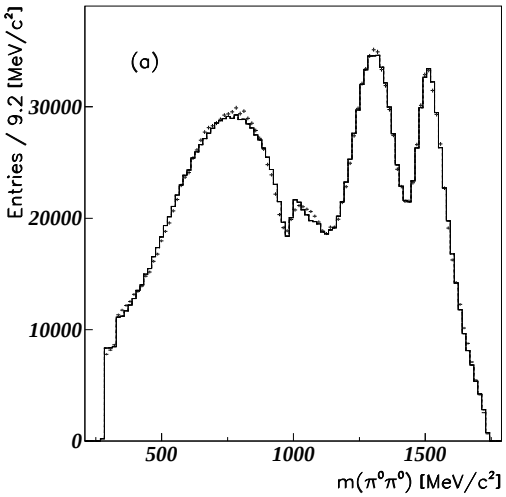

Figure 4:
The $\pi^0\pi^0$ projection, data and fit shown together.

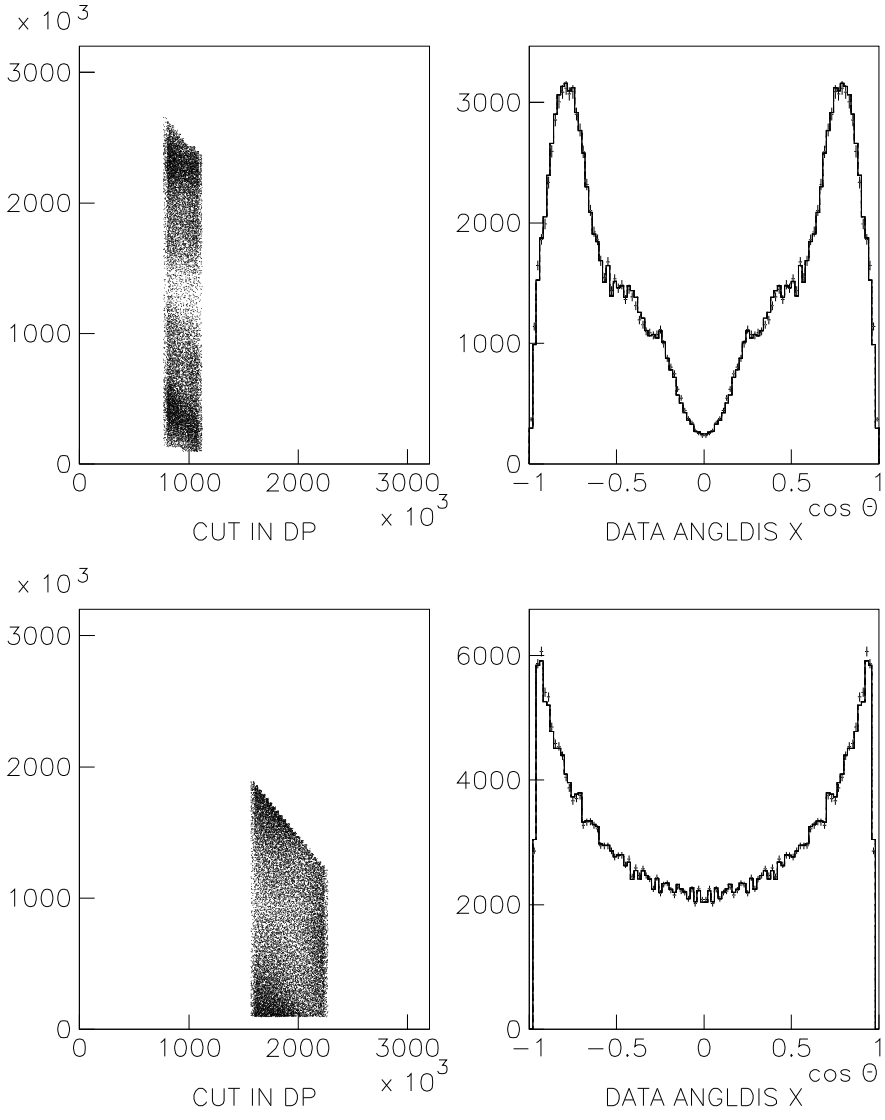
x 10 3
3000
2000
1000
0
0
1000
2000
3000
x 10 3
CUT IN DP
3000
2000
1000
0
−1
−0.5
0
0.5
1
cos Θ
DATA ANGLDIS X
x 10 3
3000
2000
1000
0
0
1000
2000
3000
x 10 3
CUT IN DP
6000
4000
2000
0
−1
−0.5
0
0.5
1
cos Θ
DATA ANGLDIS X

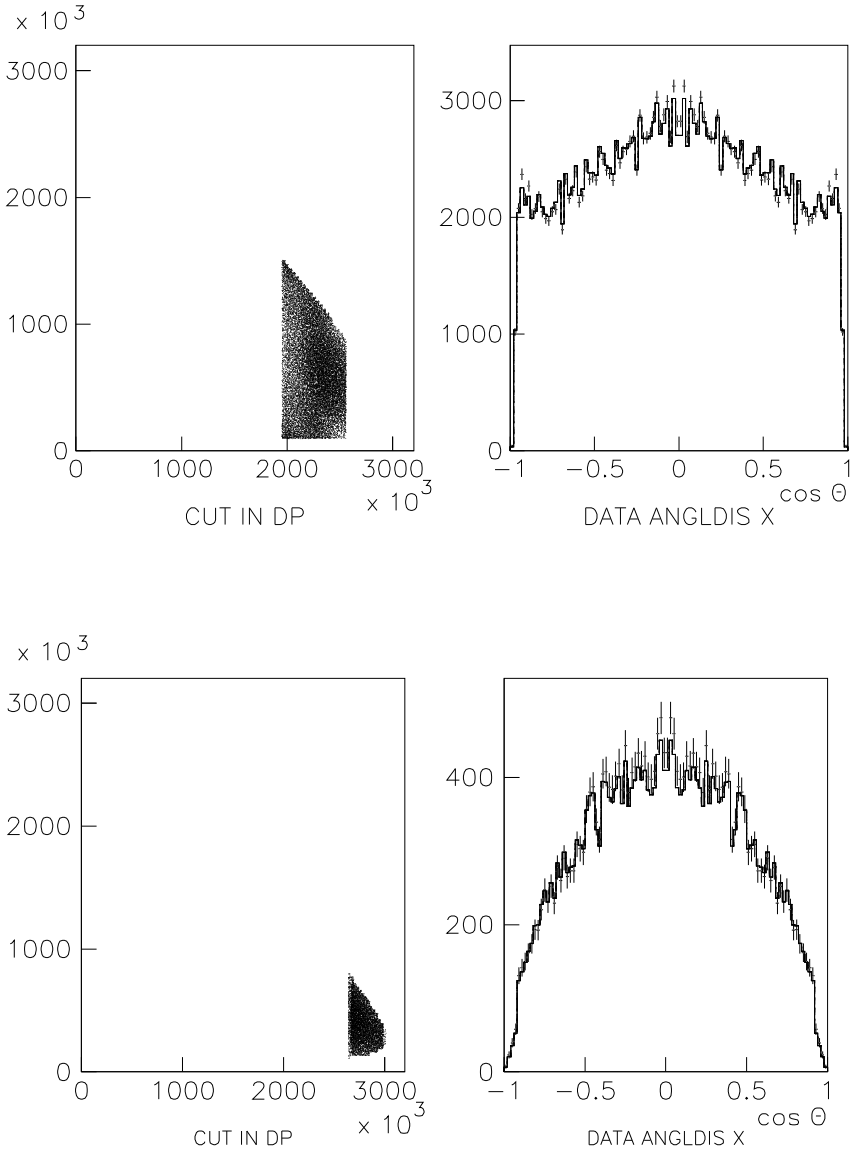

Figure 5: Symmetrized angular distributions at different mass cuts through the Dalitz plot, data and fit shown together.

4.2 $\pi^0\pi^0\eta$

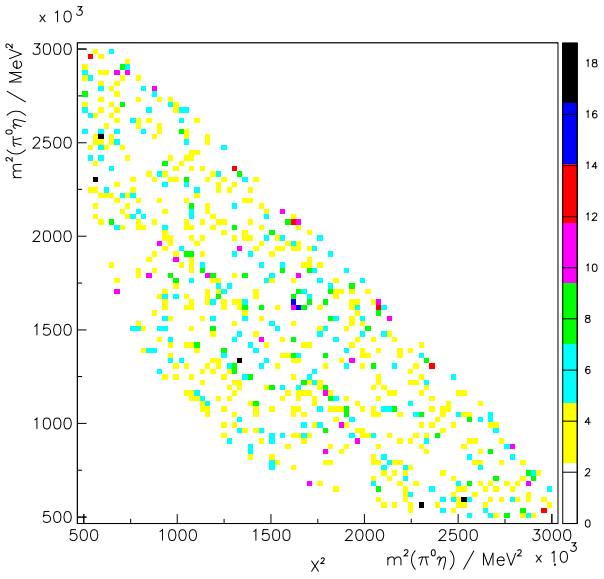

Figure 6:
The chisquare-plot for $\pi^0\pi^0\eta$.

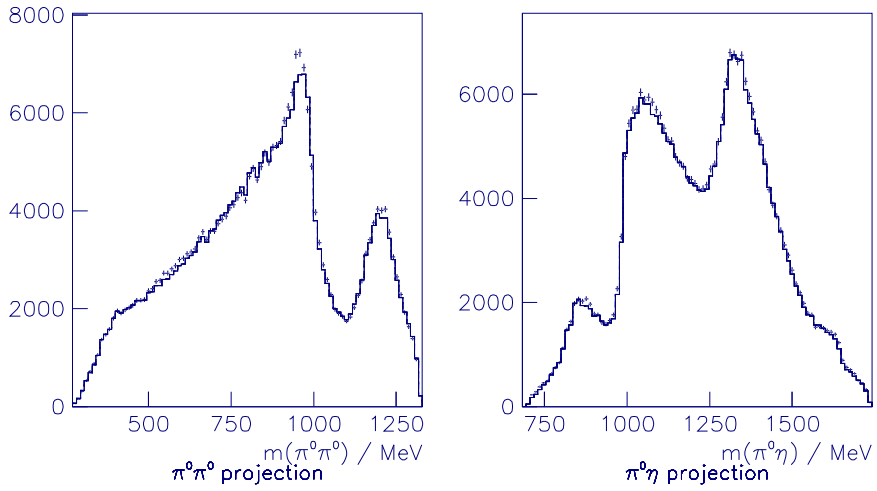

Figure 7: The $\pi^0\pi^0$ and $\pi^0\eta$ projection, data and fit displayed together.

Fig. 6 shows that the sharp $f_0(980)$ peak is not fully described. The mass position of the $f_0(980)$ is very well fixed by the phase shift of the scattering data. Apart from the different resolutions in the data samples the f_0 appears as a dip or as a bump. The different structures with slightly different mass positions have to be brought together.

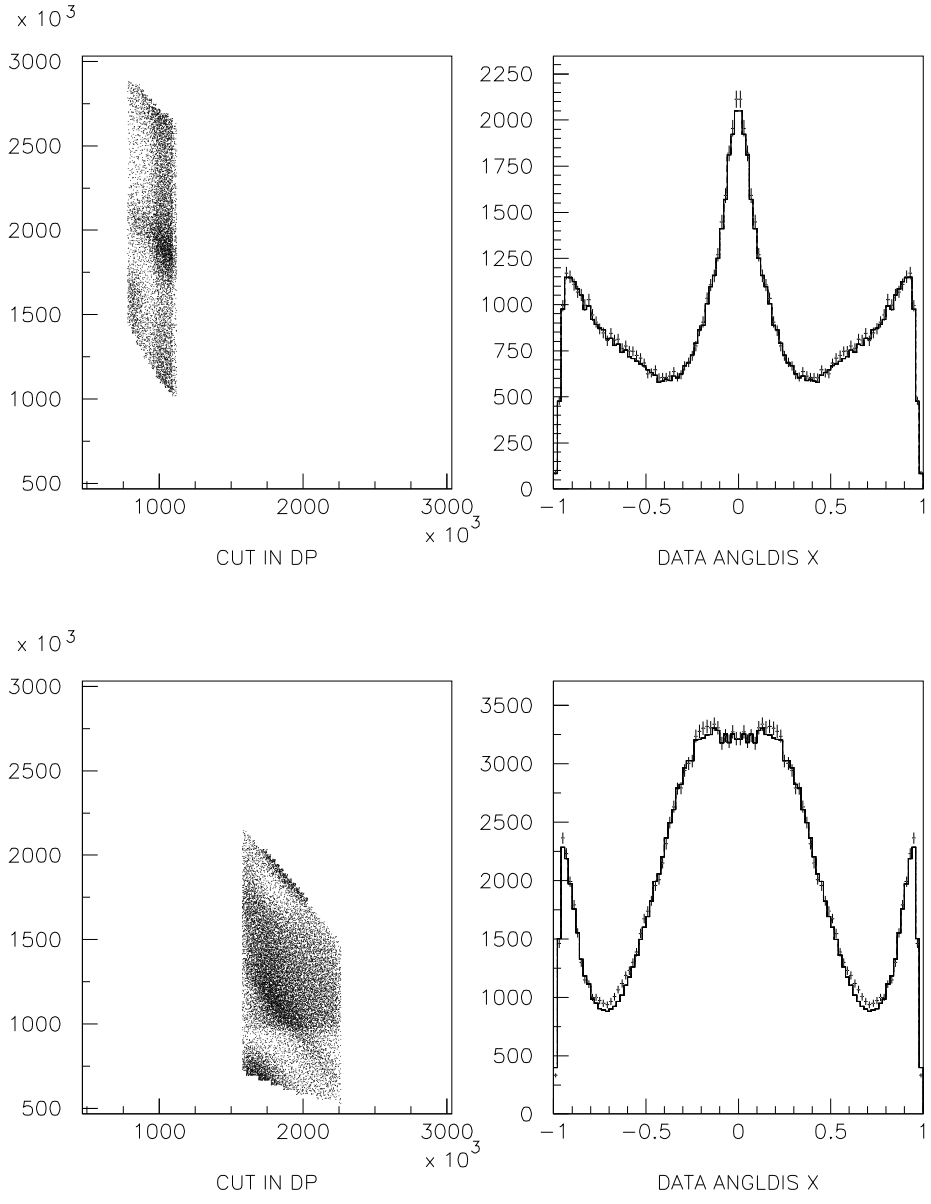

Figure 8: Cuts through the $\pi^0\pi^0\eta$ Dalitz plot at different mass positions.

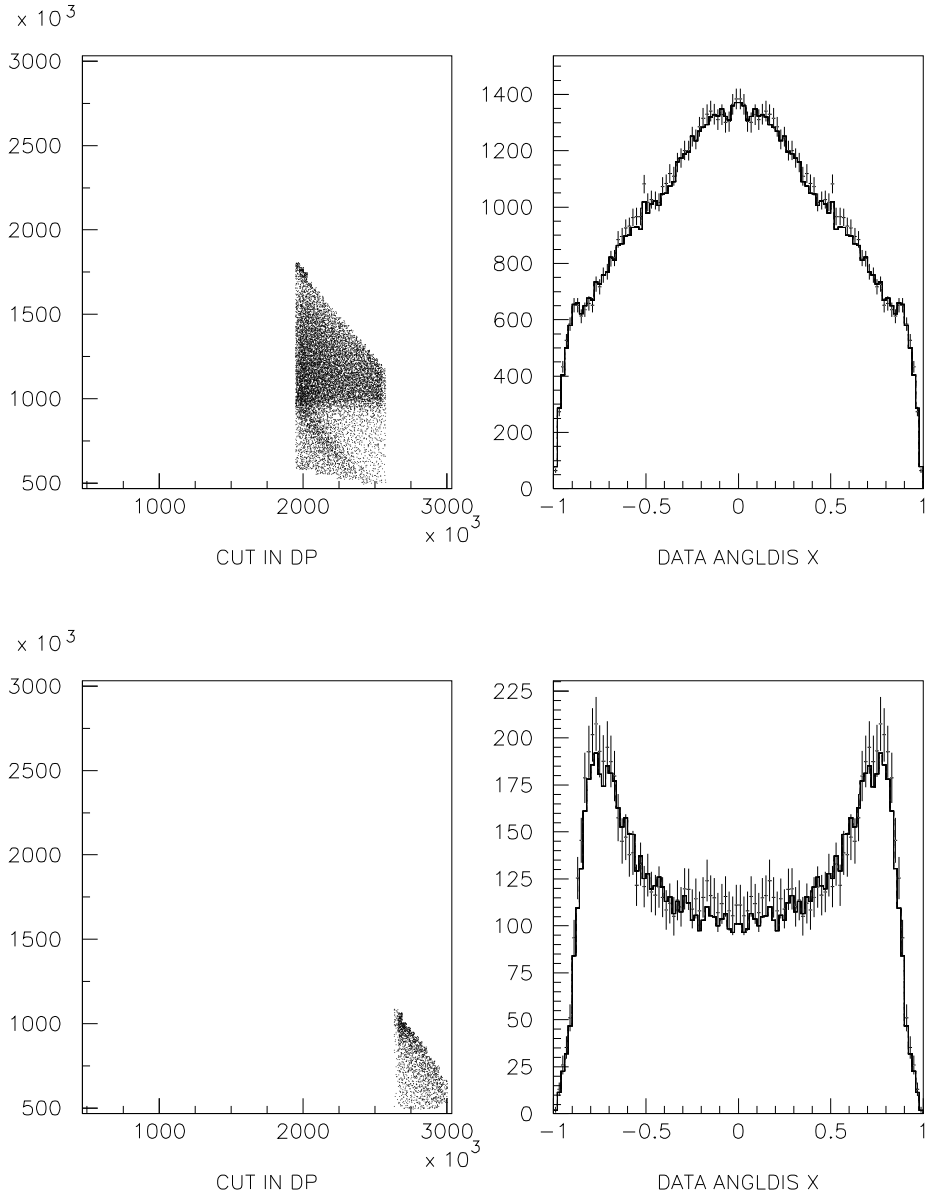

Figure 9: Cuts through the $\pi^0\pi^0\eta$ Dalitz plot at different mass positions.

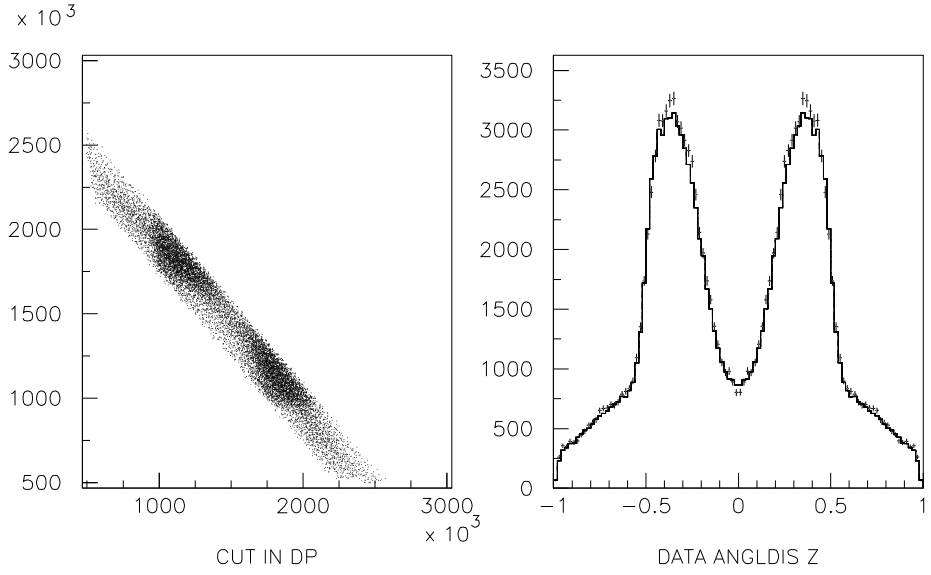

Figure 10: Cuts through the $\pi^0\pi^0\eta$ Dalitz plot at different mass positions.

4.3 $\pi^0\eta\eta$

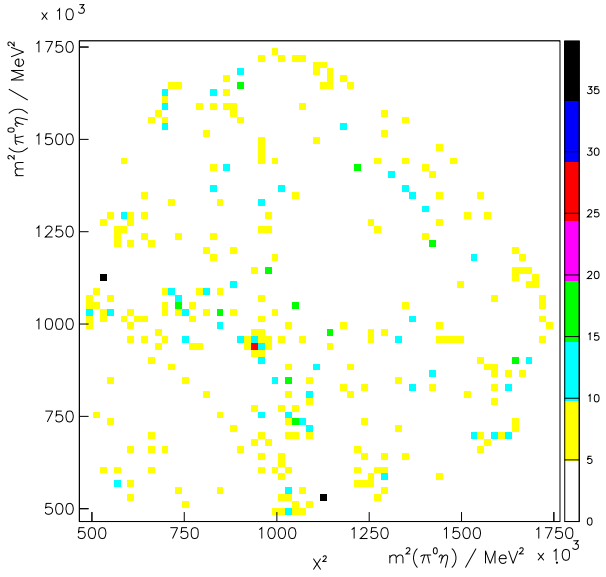

Figure 11:
The chisquare-plot for $\pi^0\eta\eta$.

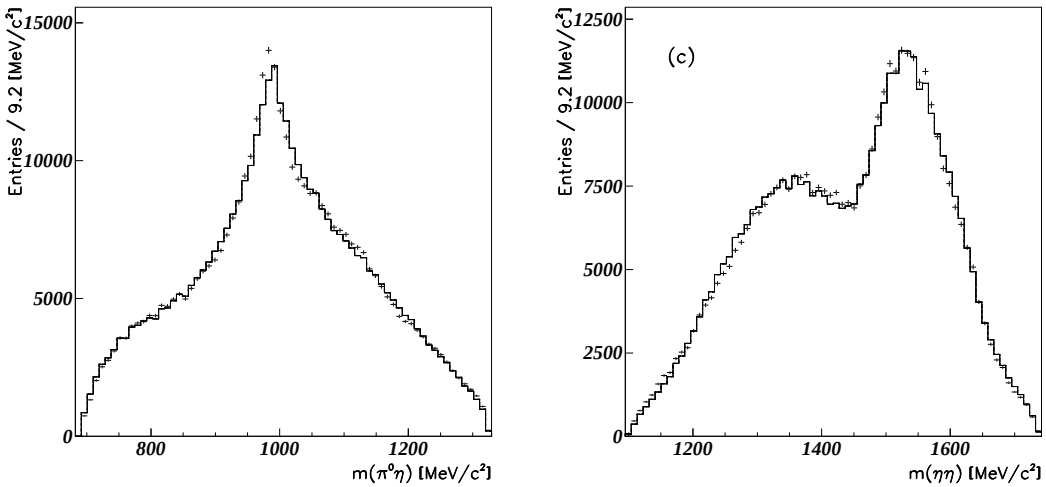

Figure 12: The $\pi^0\eta$ and $\eta\eta$ projection, data and fit displayed together.

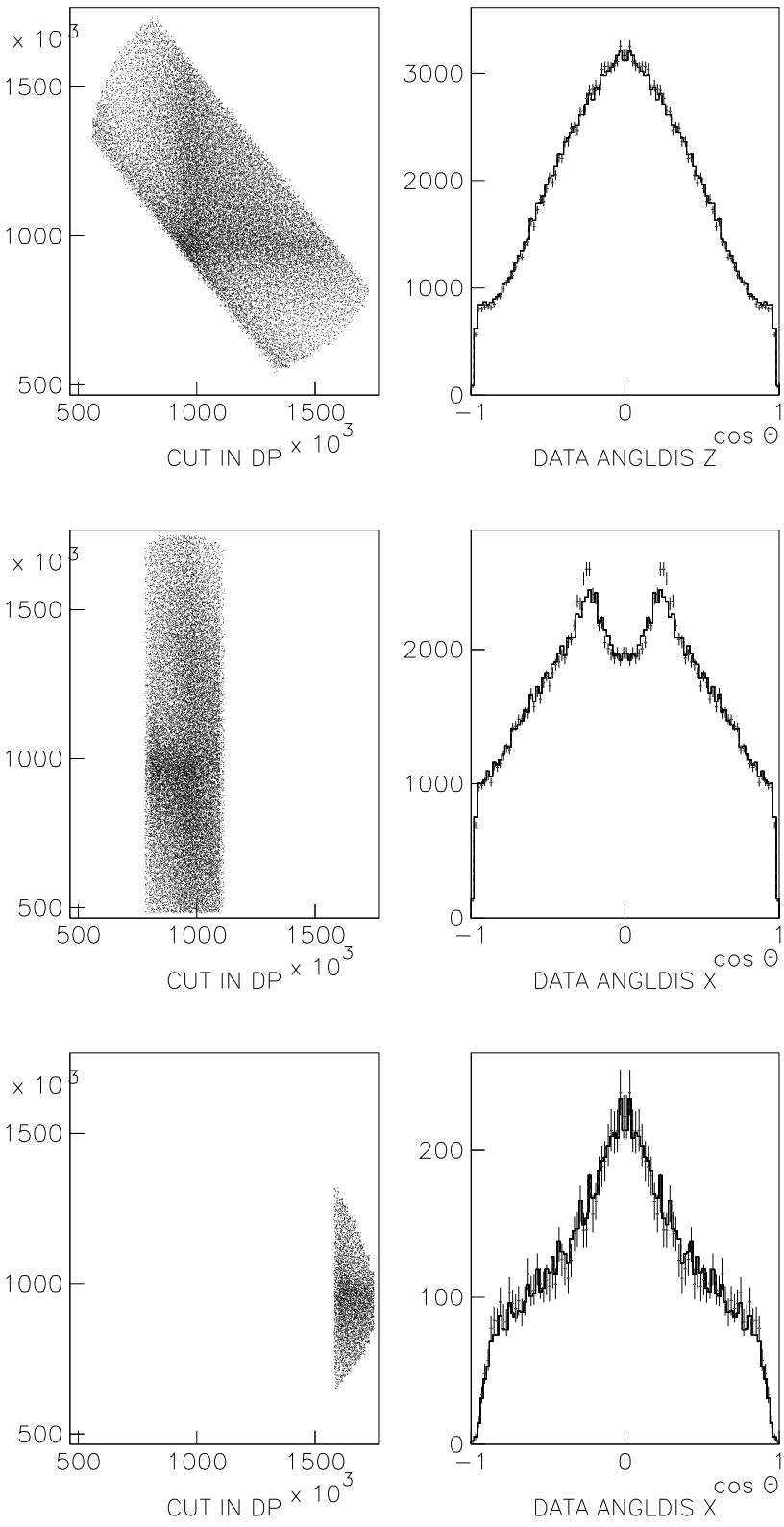

Figure 13: Cuts through the Dalitz plot at different mass positions.

4.4 Scattering data

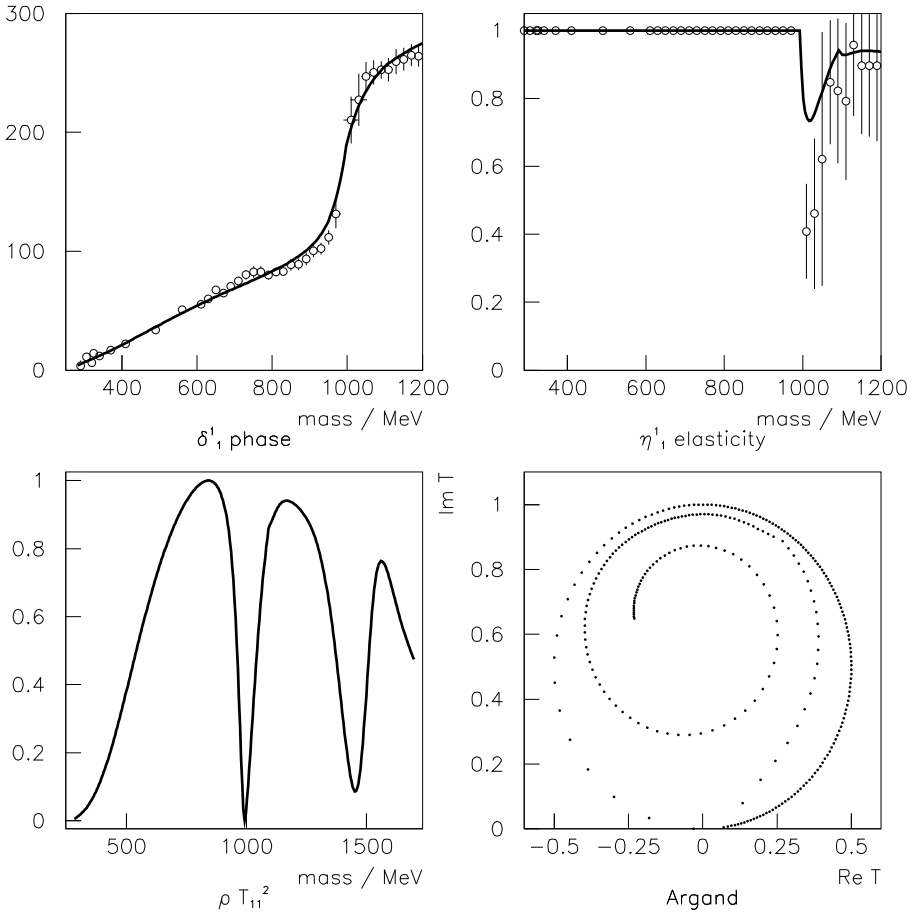

Figure 14: The $\pi\pi$ scattering data. Phase and elasticity are fitted together with the $\bar{p}p$ annihilation data. In the second column for the scattering amplitude squared and the Argand plot already the extrapolation beyond 1.2 GeV is shown.

5 Fit result

	wave	contribution [%]
$\pi^0\pi^0\pi^0$	$\pi\pi$ S–wave	76.5±5.0
	$\pi\pi$ D–wave	23.5±5.0
$\pi^0\pi^0\eta$	$\pi\pi$ S–wave	49.7±4.0
	$\pi\eta$ S–wave	16.3±3.0
	$\pi\eta$ P–wave	1.4±0.7
	$\pi\eta$ D–wave	32.6±2.5
$\pi^0\eta\eta$	$\eta\eta$ S–wave	85.8±4.0
	$\eta\eta$ D–wave	4.3±1.6
	$\pi\eta$ S–wave	9.7±2.2
	$\pi\eta$ D–wave	0.2±0.2

Table 4: Contributions of the partial waves to the different final states.

The calculation of the contributions was done as usual [8] by integration of the partial wave over the Dalitz plot and normalization to the total number of entries. In the $\pi^0\eta\eta$ Dalitz plot a fraction of 4.2% of incoherent background can be found in the fit, if one allows an additional constant. In that case the intensity is dominantely taken from the $\eta\eta$ S–wave, which reduces then to 81.9% . In the following the K–matrix parameters and production parameters are given. The extraction of the physical poles is done according to [18].

5.1 $I = 0$ S-wave

α poles	m_α [MeV/c^2]	$\tilde{\Gamma}_{\alpha\pi\pi}$ [MeV/c^2]	$\tilde{\Gamma}_{\alpha K\bar{K}}$ [MeV/c^2]	$\tilde{\Gamma}_{\alpha\eta\eta}$ [MeV/c^2]
1	841^{+5}_{-21}	666^{+12}_{-10}		
2	1169^{+10}_{-30}	691^{+100}_{-40}	21^{+30}_{-10}	
3	1240^{+10}_{-10}	3^{+1}_{-1}	13^{+6}_{-3}	316^{+6}_{-8}
4	1559^{+3}_{-4}	226^{+5}_{-5}	39^{+3}_{-5}	
	$c_{11} = c_{22} = 0$; $c_{12} = 1.082\pm0.02$			

Table 5: The K–matrix parameters of the best fit using the P–vector approach. The errors show the fluctuation in the different fits.

α pole	β_α	ϕ_α [rad]	ϕ_α [rad]	contribution [%]		
		$3\pi^0$, $\pi^0\eta\eta$	$\pi^0\pi^0\eta$	$3\pi^0$	$\pi^0\eta\eta$	$\pi^0\pi^0\eta$
1	18.2^{+4}_{-3}	0.00	0.00			
2	19.0^{+2}_{-5}	$0.22^{+0.01}_{-0.01}$	$1.2^{+0.2}_{-0.3}$	56.2±11.2	51.4±10.3	49.7±4.0
3	29.0^{+2}_{-4}	$7.09^{+0.04}_{-0.03}$	$14.3^{+2.2}_{-1.3}$			
4	35.2^{+1}_{-3}	$-5.27^{+0.02}_{-0.02}$		20.5±4.1	30.2±6.0	

Table 6: The production parameters of the $I = 0$ S–wave for the common description of $3\pi^0$ and $\pi^0\eta\eta$. The errors show the fluctuation in the different fits.

Here the 3×3 K–matrix was used. It is the result of a series of tests with different combinations of couplings and pole positions. In the presented form correlations between the parameters are kept at a minimum. The $\pi\pi$ S–wave as it is found in the $3\pi^0$ Dalitz plot is shown in fig. 17.

In a three-channel problem resonances show up as poles in three of the possible eight different Riemann sheets of the complex energy plane. The numbering of the Riemann sheets follows [19]. The relevant sheet of a pole depends on its position to the threshold it couples to. The situation is shown in fig. 18. In the isoscalar S–wave one finds pole positions listed in table 7 .

Table 7: S–wave pole positions (in MeV) in the three relevant Riemann sheets

Riemann sheet	II	III	IV
Sign convention	- + +	- - +	- - -
	996 - i56	953 - i55	938 - i35
	400 - i500	1100 - i137	1112 - i144
	1371 - i121	1407 - i167	1389 - i190
	1508 - i80	1501 - i83	1499 - i77

The second pole shows very different pole positions in the sheets II and III. By varying the sign of the $\bar{K}K$ breakup momentum one connects these two entries. This indicates that both poles belong to the same object. The behaviour of the pole is a sign that it cannot be interpreted as a Breit-Wigner resonance. The pole may be identified with a very wide background resonance $f_0(1000)$ suggested in [20]. Here the authors did an extensive study of data on the $\pi\pi$ S–wave in a limited region around the $\bar{K}K$- threshold (0.87 to 1.1 GeV).

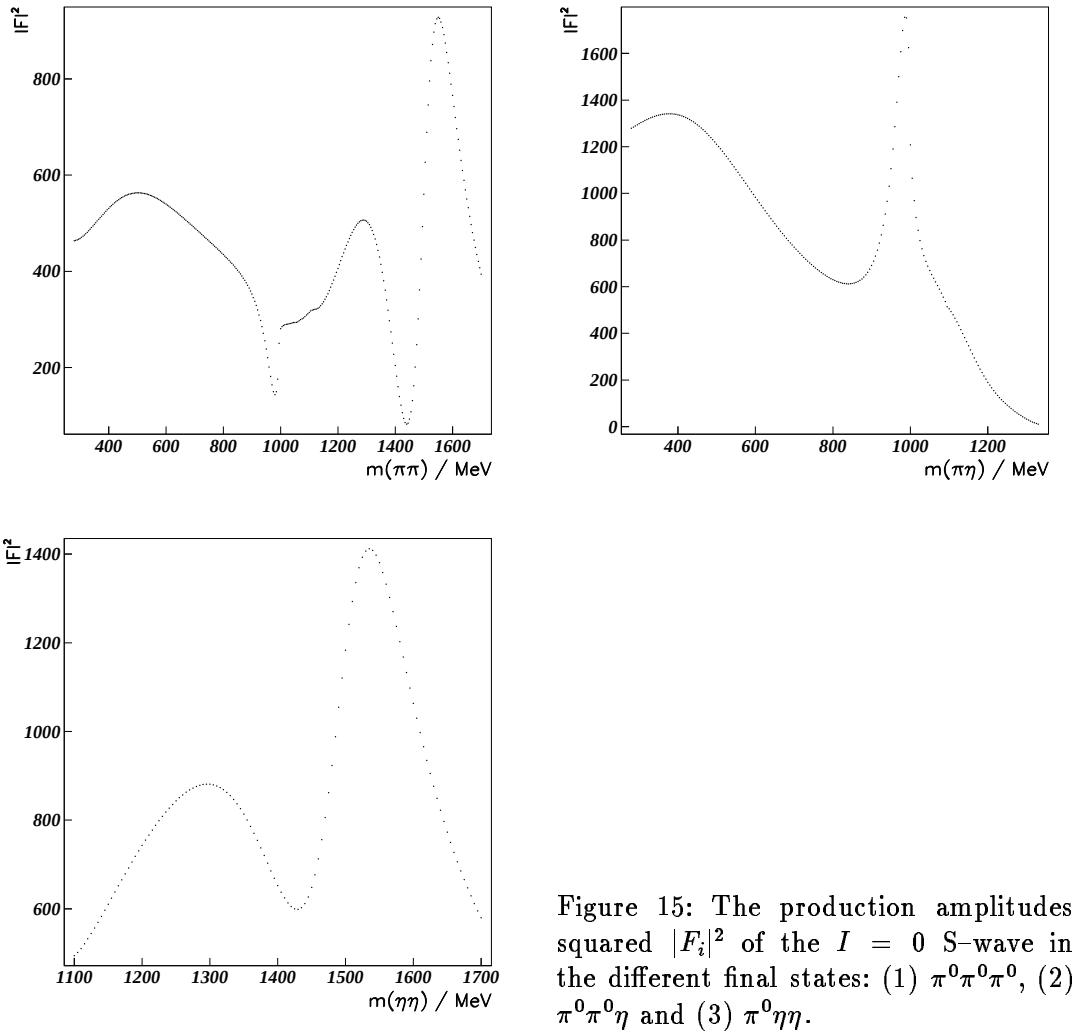

Figure 15: The production amplitudes squared $|F_i|^2$ of the $I = 0$ S–wave in the different final states: (1) $\pi^0\pi^0\pi^0$, (2) $\pi^0\pi^0\eta$ and (3) $\pi^0\eta\eta$.

The results on $f_0(1500)$ appear stable against different parametrizations and combinations of the partial wave amplitudes. It also shows a well separated intensity distribution from the rest of the $I = 0$ S–wave. Its contribution to the $3\pi^0$ and $\pi^0\eta\eta$ Dalitz plot is calculated by integration of the amplitude, which based on the 3×3 K–matrix in two steps: First, the production of the remaining S–wave poles (1,2,3) is set to zero and in the second step the wave without production of the $f_0(1500)$ is integrated over the phase space. The difference between the sum of the contributions and the total contributions of the S–wave is a measure of the error.

5.2 $I = 0$ D–wave

The $I = 0$ D–wave was fitted separately for $\pi^0\pi^0\pi^0$ and $\pi^0\eta\eta$. For the application to $3\pi^0$ a 1×1 K–matrix was used. The amplitude of the D–wave in the Dalitz plot is shown in fig. 19.

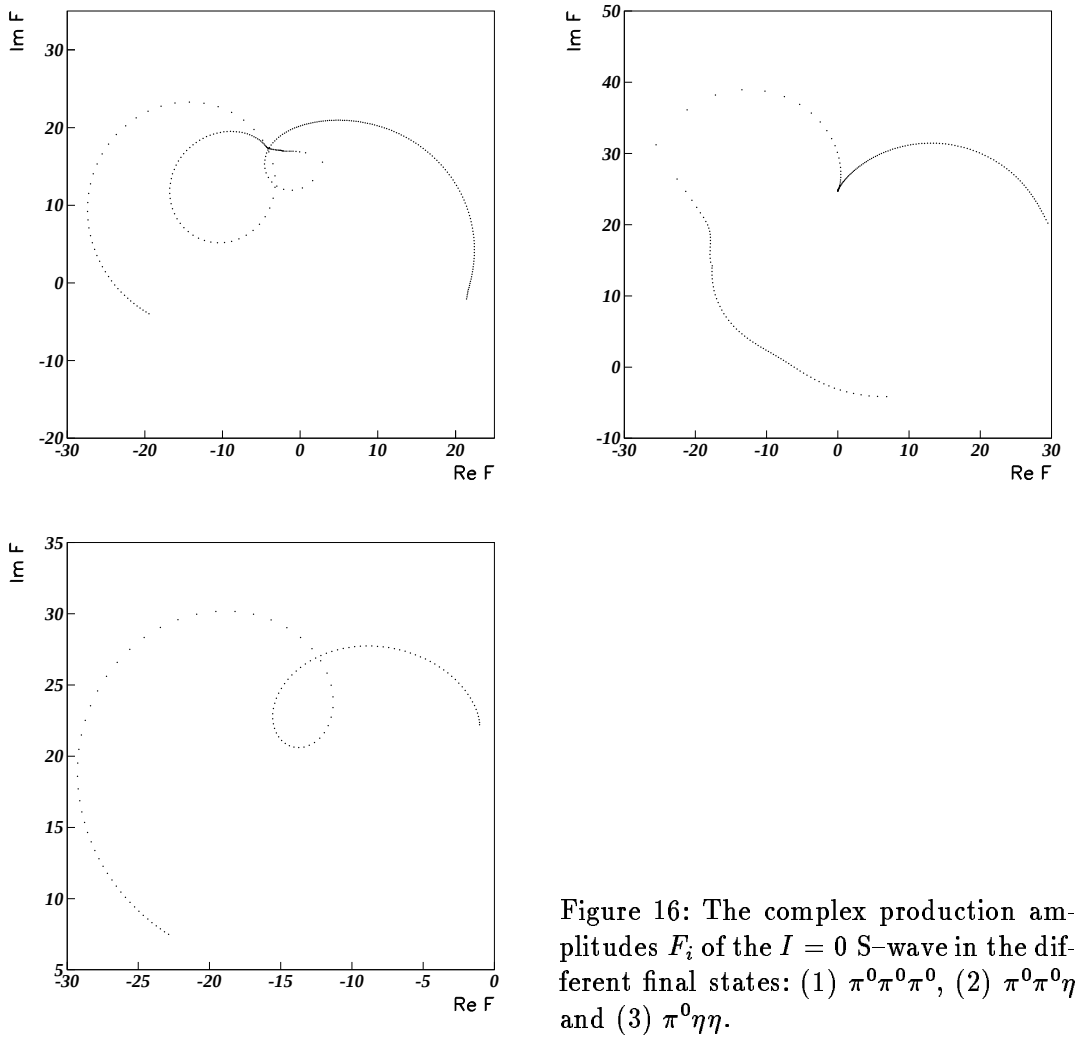

Figure 16: The complex production amplitudes F_i of the $I = 0$ S–wave in the different final states: (1) $\pi^0\pi^0\pi^0$, (2) $\pi^0\pi^0\eta$ and (3) $\pi^0\eta\eta$.

The physical pole positions are $f_2(1270)$: $(1268 - i89)\,\mathrm{MeV}/c^2$ and $f_2(1540)$: $(1552 - i71)\,\mathrm{MeV}/c^2$. The corresponding K–matrix parameters are given in table 8 .

Table 8: The K–matrix parameters of the $\pi\pi$ D–wave

α poles	m_α [MeV/c^2]	$\tilde{\Gamma}_{\alpha\pi\pi}$ [MeV/c^2]	β_α	ϕ_α [rad]	contribution [%]
1	1242^{+1}_{-1}	180^{+2}_{-3}	-30.9^{+2}_{-5}	$-1.91^{+0.01}_{-0.02}$	9.6±2.9
2	1574^{+4}_{-5}	143^{+5}_{-5}	24.0^{+2}_{-4}	$8.96^{+0.02}_{-0.02}$	13.9±4.2

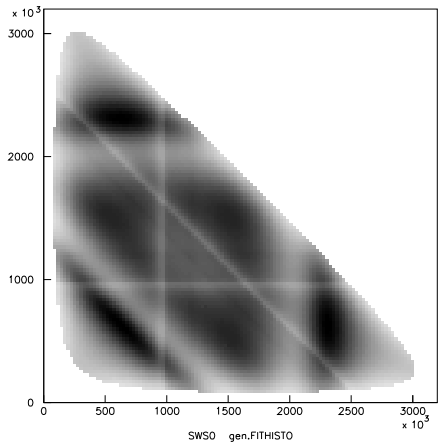

Figure 17:
The generic plot of the $\pi\pi$ S-wave.

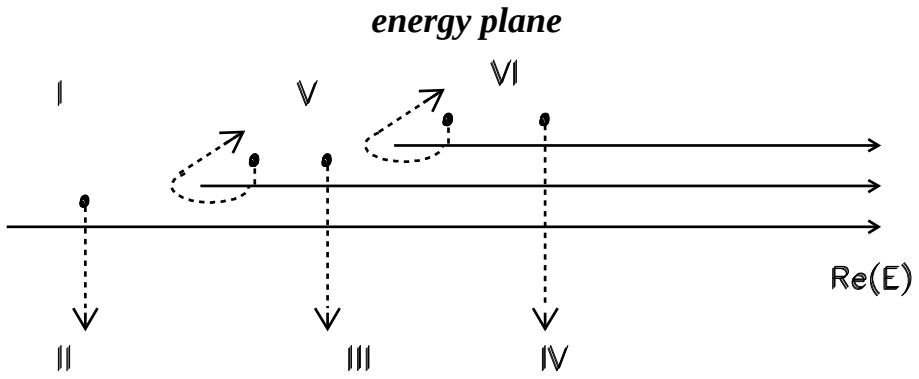

Figure 18: Complex energy plane for three open channels. The shortest path to the physical plane is drawn from different positions.

Table 9: The K–matrix parameters of the $\eta\eta$ D–wave

α poles	m_α [MeV/c^2]	$\tilde{\Gamma}_{\alpha\eta\eta}$ [MeV/c^2]	β_α	ϕ_α [rad]	contribution [%]
1	1515^{+15}_{-8}	328^{+30}_{-10}	10.2^{+1}_{-1}	$5.19^{+0.05}_{-0.03}$	4.3± 1.6

5.3 $I = 1$ waves

The $\pi\eta$ S, P and D–wave are discussed in length in[8, 10]. On the $\pi^0\pi^0\eta$ they do change marginal.

The $\pi\eta$ S–wave is fitted simultaneously to $\pi^0\pi^0\eta$ and $\pi^0\eta\eta$. The main information

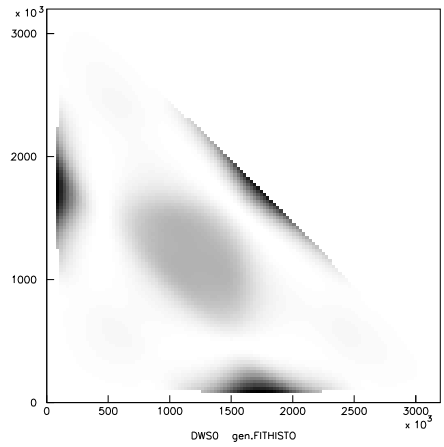

Figure 19:
The generic plot of the $\pi\pi$ D-wave.

comes from the former data sample due to phase space limitations. Production of $a_0(1470)$ in $\bar{\mathrm{p}}\mathrm{p}$ annihilation at rest into $\pi^0\eta\eta$ is therefore improbable. The common K–matrix is given in table 10 .

Table 10: The K–matrix parameters of the $\pi\eta$ S–wave

α poles	m_α [MeV/c^2]	$\tilde{\Gamma}_{\alpha\pi\eta}$ [MeV/c^2]	$\tilde{\Gamma}_{\alpha\bar{\mathrm{K}}\mathrm{K}}$ [MeV/c^2]	contribution [%]	
1	$995.4^{+0.2}_{-0.2}$	92^{+2}_{-3}	$0.8^{+0.1}_{-0.1}$	12.1±2.0	9.2±3.0
2	1490^{+10}_{-20}	18^{+2}_{-10}	213^{+23}_{-9}	4.0±1.5	0.5±0.4

On the $\pi^0\eta\eta$ the $\pi\eta$ D–wave in the presented hypothesis has very little intensity. In this plot it improved the χ^2 by an amount of 140. It is coupled via the $a_2(1320)$ on $\pi^0\pi^0\eta$ where it has high intensity. Therefore its parameters are determined from this data ($M = 1315 \pm 5$, $\Gamma = 112 \pm 5$).

6 Summary

From the diameter in the Argand plot fig. 20 one obtains a partial width to $\pi^0\pi^0$ of $0.76 \cdot 135\,\mathrm{MeV} = 102.6\,\mathrm{MeV}$ at the mass position of 1500 MeV. Remember, the partial $\bar{\mathrm{K}}\mathrm{K}$ width accounts for further open channels. The $\eta\eta$ width plus width of unconsidered channels at 1500 MeV is 32.4 MeV.

The following table lists the averages for the mass and width of $f_0(1500)$ obtained in the individual investigations and in the coupled channel fit. The errors assigned to the mass and width are obtained in the separate fits. From the contribution of the $f_0(1500)$ to the different final states $3\pi^0$, $\pi^0\eta\eta$ and $\pi^0\eta\eta'$ one is able to calculate the relative couplings to the channels $\pi^0\pi^0$, $\eta\eta$ and $\eta\eta'$.

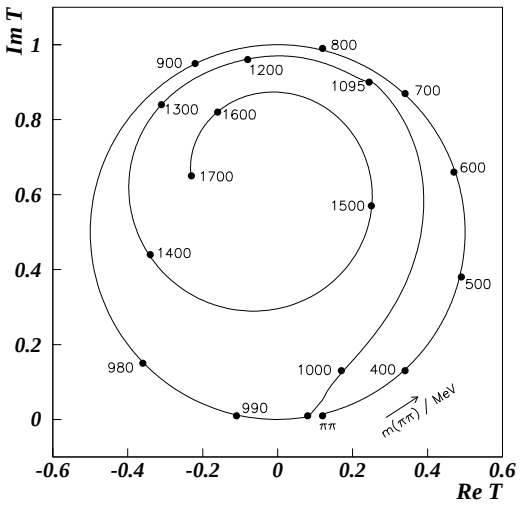

Figure 20: The Argand plot obtained from the simultaneous fit to $\pi^0\pi^0\pi^0$, $\pi^0\pi^0\eta$ and $\pi^0\eta\eta$ final states of $\bar{p}p$ annihilation at rest and scattering data.

channel	mass [MeV/c^2]	width [MeV/c^2]	BR $\times 10^{-3}$	$\bar{q}(f_0(1500))$ [MeV/c]
$\pi^0\pi^0$	1500± 15	120± 25	1.27±0.33	726.6
$\eta\eta$	1505± 15	120± 30	0.60±0.17	493.4
$\eta\eta'$	1545± 25	100± 40	0.16±0.04	194.7
$\bar{K}K$				(540.0)

From these numbers one calculates:

$$\pi^0\pi^0 \ : \eta\eta \ : \eta\eta' \ = 1 : 0.70 \pm 0.27 : 0.47 \pm 0.17 \qquad (19)$$

References

[1] C. Amsler et al., Phys. Lett. **B 342**(1995) 433 .

[2] C. Amsler et al., in preparation for Phys. Lett. **B** (1995) .

[3] C. Amsler et al., Phys. Lett. **B 333**(1994) 277 .

[4] I.J.R. Aitchison, Nucl. Phys. **A189**(1972) 417 .

[5] F. v. Hippel and C. Quigg, Phys. Rev.**5**(1972)624 .

[6] C. Zemach, Phys. Rev. **133**(1964) 1201, Phys. Rev. **B 140**(1965) 97, 109
P. Baillon, Use of Tensor Calculus for the Analysis of Reactions Between Elementary Particles, Ed. K. Nikolic, Gordon and Preach, Science Publ., Herzog-Novi (1968) Vol 4.2 .

[7] Ralf Hackmann, High-statistics study of $\bar{p}p$ annihilation into $\pi^0\pi^0\pi^0$ and $\pi^0\pi^0\eta$, CB-note .

[8] Stefan Spanier, Partial wave analysis of $\bar{p}p$ annihilation into $\pi^0\pi^0\eta$ at rest, CB-note 235 .

[9] Jens Brose, Technical report on the high-statistics partial wave analysis of $\bar{p}p \rightarrow \pi^0\pi^0\pi^0$ at rest in liquid hydrogen, CB-note 255 .

[10] Ralf Hackmann, Technical report of the $\pi^0\eta\eta$ analysis, CB-note 273 .

[11] G. Grayer et al., Nucl. Phys. **B 75**(1974) 189 .

[12] L. Rosselet, Phys. Rev. **D 15**(1977) 574 .

[13] S. Spanier, Parametrization of the $I = 0$ $\pi\pi$ S–wave, CB-note 227 .

[14] I. Augustin, Dissertation, Universit"at Karlsruhe (1993);
C. Amsler et al., Phys. Lett. **B 291**(1992) 347 .

[15] S. U. Chung et al. , Partial wave analysis in K-matrix formalism, *submitted to Ann.Phys.* .

[16] C. Amsler et al., Phys. Lett. **B 297**(1992) 214 .

[17] F. James and M. Roos, CERN Program Library (1989) D506,
CERN Computer Centre, Geneva. .

[18] S. Spanier, Resonance-Parameters, CB-Note 230 .

[19] W.R. Frazer, A.W. Hendry, Phys.Rev. **134**(1964)B 1307 .

[20] D.Morgan and M.R. Pennington, Phys. Rev. **D 48**(1993) 1185 .